Atmos. Chem. Phys. Discuss., 15, 6745–6770, 2015
www.atmos-chem-phys-discuss.net/15/6745/2015/
doi:10.5194/acpd-15-6745-2015


Atmospheric Chemistry and Physics Discussions



# Simulating $CO_2$ profiles using NIES TM and comparison with HIAPER Pole-to-Pole Observations

**C. Song[1], S. Maksyutov[2], D. Belikov[2], H. Takagi[2], and J. Shu[1]**

[1]Key Laboratory of Geographic Information Science, Institute of Climate Change, East China Normal University, Shanghai 200241, China
[2]National Institute for Environmental Studies, Tsukuba 305-8506, Japan

Received: 26 January 2015 – Accepted: 28 January 2015 – Published: 6 March 2015

Correspondence to: C. Song (songci193@126.com)

Published by Copernicus Publications on behalf of the European Geosciences Union.







## Abstract

We present a study on validation of the National Institute for Environmental Studies Transport Model (NIES TM) by comparing to observed vertical profiles of atmospheric $CO_2$. The model uses a hybrid sigma-isentropic ($\sigma$–$\theta$) vertical coordinate that employs both terrain-following and isentropic parts switched smoothly in the stratosphere. The model transport is driven by reanalyzed meteorological fields and designed to simulate seasonal and diurnal cycles, synoptic variations, and spatial distributions of atmospheric chemical constituents in the troposphere. The model simulations were run for biosphere, fossil fuel, air–ocean exchange, biomass burning and inverse correction fluxes of carbon dioxide ($CO_2$) by GOSAT Level 4 product. We compared the NIES TM simulated fluxes with data from the HIAPER Pole-to-Pole Observations (HIPPO) Merged 10 s Meteorology, Atmospheric Chemistry, and Aerosol Data, including HIPPO-1, HIPPO-2 and HIPPO-3 from 128.0° E to −84.0° W, and 87.0° N to −67.2° S.

The simulation results were compared with $CO_2$ observations made in January and November 2009, and March and April 2010. The analysis attests that the model is good enough to simulate vertical profiles with errors generally within 1–2 ppmv, except for the lower stratosphere in the Northern Hemisphere high latitudes.

## 1 Introduction

Atmospheric carbon dioxide ($CO_2$) is the primary radiative forcing greenhouse gas produced by human activities. It causes the most global warming (IPCC, 2013) and its atmospheric concentration has been increasing at a progressively faster rate each decade because of rising global emissions (Raupach et al., 2007). The monitoring of atmospheric $CO_2$ from space is intended to identify the sources and sinks of the greenhouse gases generated by human and natural activities. A number of satellites are actively monitoring greenhouse gases (e.g., GOSAT, SCIAMACHY, AIRS, IASI) to answer this question, and retrieval algorithms for $CO_2$ have been developed for these





ACPD
15, 6745–6770, 2015



satellite observation data to provide more accurate estimates of $CO_2$ concentrations using several different methods.

The sparseness and spatial inhomogeneity of the existing surface network have limited our ability to understand the quantity and spatiotemporal distribution of $CO_2$ sources and sinks (Scholes et al., 2009). Recent studies of global sources and sinks of greenhouse gases, and their concentrations and distributions, have been mainly based on in situ surface measurements (GLOBALVIEW-$CO_2$, 2010). The diurnal and seasonal "rectifier effect", the covariance between surface fluxes and the strength of vertical mixing, and the proximity of local sources and sinks to surface measurement sites all have an influence on the measured and simulated concentrations, and complicate the interpretation of results (Denning et al., 1996; Gurney et al., 2004; Baker et al., 2006). Comparatively speaking, the vertical integration of mixing ratio divided by surface pressure, denoted as the column-averaged dry-air mole fraction (DMF; denoted XG for gas G) is much less sensitive to the vertical redistribution of the tracer within the atmospheric column (e.g., due to variations in planetary boundary layer (PBL) height) and is more easily related to the underpinning surface fluxes than are near-surface concentrations (Yang et al., 2007). Thus, column-averaged measurements and simulations are expected to be very useful for improving our understanding of the carbon cycle (Yang et al., 2007; Keppel-Aleks et al., 2011; Wunch et al., 2011). In addition, atmospheric transport has to be accounted for when analyzing the relationships between observations of atmospheric constituents and their sources/sinks near the earth's surface or through the chemical transformation in the atmosphere. As a result, reliable estimates of climate change depend upon our ability to predict atmospheric $CO_2$ concentrations, which requires further investigation of the $CO_2$ sources, sinks, and atmospheric transport.

Global atmospheric tracer transport models are usually applied to studies of the global cycles of the long-lived atmospheric trace gases, such as $CO_2$ and methane ($CH_4$), because the long-lived atmospheric tracers exhibit observable global patterns (e.g., the interhemispheric gradient of the concentration). Global three-dimensional





ACPD
15, 6745–6770, 2015



chemistry transport models (hereafter referred to as CTMs), driven by actual meteorology from numerical weather predictions, and global circulation models (GCMs) play a crucial role in assessing and predicting change in the composition of the atmosphere due to anthropogenic activities and natural processes (Rasch et al., 1995; Jocob et al., 1997; Denning et al., 1999; Bregman et al., 2006; Law et al., 2008; Maksyutov et al., 2008; Patra et al., 2008).

The transport modeling is done on different scales ranging from local plume spread, regional mesoscale transport to global scale analysis, depending on the scale of the phenomena that are studied. Forward modeling is used to estimate tracer concentrations in regions that lack observation data and to identify the features of tracer transport and dispersion (Law et al., 2008; Patra et al., 2008). Inverse methods are generally applied when interpreting the data, with atmospheric transport models providing the link between surface gas fluxes and their subsequent influence on atmospheric concentrations (Rayner and O'Brien, 2001; Patra et al., 2003a, b; Gurney et al., 2004; Baker et al., 2006). Global modeling analysis has helped to identify the relative contribution of the land and oceans in the Northern and Southern Hemispheres to the interhemispheric concentration differences in $CO_2$, $CH_4$, carbon monoxide (CO) and other tracer species (Bolin and Keeling, 1963; Hein et al., 1997). For stable and slowly reacting chemical species, a number of studies have derived information on the spatial and temporal distribution of the surface sources and sinks by applying a transport model and atmospheric observations (Tans et al., 1990; Rayner et al., 1999).

There are several factors that strongly influence model performance: the numerical transport algorithm used, meteorological data, grid type and resolution. In tracer transport calculations, semi-Lagrangian transport algorithms are often used in combination with finite-volume models. Losses in the total tracer mass are possible in these algorithms. While such losses are often negligible for short-term transport simulations, they can seriously distort the global trends and tracer budgets in long-term simulations. To avoid such losses, various mass-fixing schemes have been applied (Hacket al., 1993; Rasch et al., 1995). Although the use of mass fixers can prevent mass losses, there





ACPD
15, 6745–6770, 2015



remains a possibility of predicting distorted tracer concentrations. By contrast, when using a flux-form transport algorithm, the total tracer mass is conserved and thus the issue of mass losses can be eliminated, provided the flow is conservative. The use of numerical schemes with limiters leads to distorted tracer concentrations and affects the linearity. Thus, to accurately calculate the tracer concentration in a forward simulation and to use the model in inverse modeling, we employed a flux-form version of the global off-line, three-dimensional chemical NIES TM.

The synoptic and seasonal variability in $XCO_2$ is driven mainly by changes in surface pressure, the tropospheric volume-mixing ratio (VRM) and the stratospheric concentration, which is affected in turn by changes in tropopause height. The effects of variations in tropopause height are more pronounced with increasing contrast between stratospheric concentrations. Many CTMs demonstrate some common failings of model transport in the stratosphere (Hall et al., 1999). The difficulty of accurately representing dynamical processes in the upper troposphere (UT) and lower stratosphere (LS) has been highlighted in recent studies (Mahowald et al., 2002; Wauch and Hall, 2002; Monge-Sanz et al., 2007). While there are many contributing factors, the principal factors affecting model performance in vertical transport are meteorological data and the vertical grid layout (Monge-Sanz et al., 2007).

The use of different meteorological fields in driving chemical transport models can lead to diverging distribution of chemical species in the UTLS region (Douglass et al., 1999). The quality of wind data provided by numerical weather predictions is another crucial factor for tracer transport (Jöckel et al., 2001; Stohl et al., 2004; Bregman et al., 2006). Wind fields produced by the Data Assimilation System (DAS) are commonly used for driving CTMs. Spurious variability, or "noise", introduced via the assimilation procedure affects the quality of meteorological data through a lack of suitable observations, or by the inaccurate treatment of model biases (Bregman et al., 2006). This negative effect is proportional to the dynamic time scale and increases with operational time. The most sensitive area in this regard is the lower stratosphere in tropical regions, where large volumes of air move upward from the troposphere to the strato-





ACPD
15, 6745–6770, 2015



sphere. A lack of observations makes this region the most challenging in terms of data assimilation. Bregman et al. (2006) found that the modeled vertically integrated mass change obtained for the tropical atmosphere is not in geostrophic balance with the surface pressure tendency. Schoeberl et al. (2003) suggested that GEOS DAS (Geodetic Earth Orbiting Satellite Data Assimilation System) is less suitable for long-term stratospheric transport studies than wind from a general circulation model. At the same time, improvements to the data assimilation system itself (ECMWF ERA-Interim reanalysis; Dee and Uppala, 2009) and the development of special products for use in transport models (MERRA: Modern Era Retrospective-analysis for Research and Applications; Bosilovich et al., 2008) have assisted in improving the accuracy of atmospheric circulation when using off-line models (Monge-Sanz et al., 2007).

Belikov et al. (2013) evaluated the simulated column-averaged dry air mole fraction of atmospheric carbon dioxide ($XCO_2$) against daily ground-based high-resolution Fourier Transform Spectrometer (FTS) observations measured at twelve sites of the Total Column Observing Network (TCCON), which provides an essential validation resource for the Orbiting Carbon Observatory (OCO), SCIAMACHY, and GOSAT. In this manuscript, we present the application of the standard isentropic troposphere version transport model with HIAPER Pole-to-Pole Observations (HIPPO) Merged 10 s Meteorology, Atmospheric Chemistry, and Aerosol Data, which are highly time-resolved, because of the underlying 1 s in situ frequency measurement, and vertically-resolved, because of the GV flight plans that performed 787 vertical ascents/descents from the ocean/ice surface up to the tropopause. The remainder of this paper provides the model information and a detailed description of the meteorology dataset and HIPPO data, and a validation of the $CO_2$ vertical profiles comparing against the HIPPO observations, followed by a discussion and conclusions.





ACPD
15, 6745–6770, 2015



## 2 Model features and operation

In this section, we describe the features and use of the NIES TM (denoted NIES-08, Ii). As Belikov et al. (2011, 2013) described, the latest improved version of the NIES TM model uses the ($\theta$–$\sigma$) hybrid sigma-isentropic vertical coordinate that is isentropic in the UTLS region but terrain-following in the free troposphere. This designed coordinate helps to simulate vertical motion in the isentropic part of the grid above level 350 K. Basic physical model features include the flux-form dynamical core with a third-order van Leer advection scheme, a reduced latitude–longitude grid, a horizontal flux-correction method for mass balance, and turbulence parameterization.

### 2.1 Meteorological data used in the simulation

The NIES TM is an off-line model driven by Japanese reanalysis data, which covers more than 30 years from 1 January 1979 to present (Onogi et al., 2007). The period of 1979–2004 is covered by the Japanese 25 year Reanalysis (JRA-25), used by Belikov et al. (2013), and is the product of the Japan Meteorological Agency (JMA) and Central Research Institute of Electric Power Industry (CRIEP). After 2005, real-time operational analysis, employing the same assimilation system as JRA-25, has been continued as the JMA Climate Data Assimilation System (JCDAS). The JRA-25/JCDAS dataset is distributed on a Gaussian horizontal grid T106 (320 × 160) with 40 hybrid $\sigma$–p levels. The 6 hourly time step of JRA-25/JCDAS is coarser than the 3 hourly data from the National Centers for Environmental Prediction (NCEP) Global Forecast System (GFS) and Global Point Value (GPV) datasets, which were used in the previous model version (Belikov et al., 2011). However, with a better vertical resolution (40 levels on a hybrid $\sigma$-p grid vs. 25 and 21 pressure levels for GFS and GPV, respectively) it is possible to implement a vertical grid with 32 levels (vs. the 25 levels used before), resulting in a more detailed resolution of the boundary layer and UTLS region (Table 1).

The 2-D monthly distribution of the climatological heating rate, used to calculate vertical transport in the $\theta$-coordinate domain of the hybrid sigma-isentropic coordinate,





ACPD
15, 6745–6770, 2015



is prepared from JCDAS reanalysis data, which are provided as the sum of short- and long-wave components on pressure levels.

### 2.2 HIPER Pole-to-Pole data

The HIPPO study investigated the carbon cycle and greenhouse gases at various altitudes (from 0 to 16 km) in the western hemisphere through the annual cycle. HIPPO is supported by the National Science Foundation (NSF) and its operations are managed by the Earth Observing Laboratory (EOL) of the National Center for Atmospheric Research (NCAR). Its base of operations is the EOL Research Aviation Facility (RAF) at the Rocky Mountain Metropolitan Airport (RMMA) in Jefferson Country, Colorado. The main goal of HIPPO was to determine the global distribution of $CO_2$ and other trace atmospheric gases by sampling at several altitudes and latitudes (from 0 to 16 km, 87.0° N to −67.2° S) in the Pacific Basin.

The dataset used in this paper includes the merged 10 s data product of meteorological, atmospheric chemistry, and aerosol measurements from three HIPPO Missions 1 to 3. The three missions took place from January 2009 to April 2010; HIPPO-1 (9–26 January 2009), HIPPO-2 (2–22 November 2009), and HIPPO-3 (24 March–15 April 2010), ranging from 128.0° E to −84.0° W, and 87.0° N to −67.2° S (Table 2). All data are provided in a single space-delimited format ASCII file (https://www.eol.ucar.edu/field_projects/hippo).

HIPPO measured atmospheric constituents along transects running approximately pole-to-pole over the Pacific Ocean and recorded hundreds of vertical profiles from the ocean/ice surface up to the tropopause five times during four seasons from January 2009 to September 2011. HIPPO provides the first high-resolution vertically resolved global survey of a comprehensive suite of atmospheric trace gases and aerosols pertinent to understanding the carbon cycle and challenging global climate models. The 10 s merge product applied in this study was derived by combining the National Science foundation (NSF)/NCAR GV aircraft navigation and atmospheric structure parameters including position, time, temperature, pressure, and wind speed reported at





ACPD
15, 6745–6770, 2015



1 s frequency, with meteorological, atmospheric chemistry and aerosol measurements made by several teams of investigators on a common time and position basis.

### 2.3 Model setup

The standard model was run with the three HIPPO missions to study atmospheric tracer transport and the ability of the model to reproduce the column-averaged dry air mole fractions and vertical profile of atmospheric $CO_2$. The model was run with a 6 h time step and 1° space step at a horizontal resolution of 2.5° × 2.5° and 32 vertical levels from the surface to 3 hPa using tracer $CO_2$.

The $CO_2$ simulations were began on 1 January 2009, 1 November 2009 and 1 March 2010 for the three HIPPO missions 1 to 3, respectively, with individual initial 3-D tracer distributions using the Level 4A global fluxes of biosphere–atmosphere, fossil fuel, air–ocean exchange, biomass burning, and inverse correction, obtained by monthly global $CO_2$ flux estimated from FTS (SWIR) level 2 $XCO_2$ data.

## 3 Discussions

The current model versions have been used in several tracer transport studies and were evaluated through participation in transport model intercomparisons (Niwa et al., 2011; Patra et al., 2011). The simulation results of the tracer transport model show good consistency with observations in the near-surface layer and in the free troposphere. However, the model performance in the UTLS region has not been evaluated in detail.

### 3.1 Comparison with $CO_2$ observations

Figure 1 show the scatters diagram of modeled results vs. total column of HIPPO-1, 2, 3. The majority of points are within a 95 % confidence interval of total $CO_2$ column





ACPD
15, 6745–6770, 2015



concentration. Modeled HIPPO-1's precision successively exceeds 2 and 3, inferring the simulation results with the relevant either seasonal changes or data quality.

The simulation results of $CO_2$ concentration time-varying for HIPPO-1 using the standard model display good performance and weak dispersion of concentrations. The validation results (Fig. 2a) show that approximately 69.2 % of the absolute biases are within 1 ppmv, approximately 92.3 % are within 2 ppmv, and only 7.7 % exceed 3 ppmv. Furthermore, as shown by the root-mean-square error (RMSE) with time, during most days in January the model values were stable compared with the observed values, apart from the first few days of the month. According to the simulation results of the HIPPO-1 observed and simulated latitude-varying $CO_2$ concentration data, the comparison values always underestimate the atmospheric $XCO_2$, and the differences are all within 1.5 ppmv in the Southern Hemisphere, and vice versa in the Northern Hemisphere with 85.8 % of the differences under 1.1 ppmv. Figure 2b shows that the larger biases usually occur in the Northern Hemisphere high latitudes. The RMSE also reflects the instability of the simulated values in the Northern Hemisphere high latitudes.

For HIPPO-2 data from 2 to 22 November 2009,the absolute biases of observed and simulated time-varying are all within 2 ppmv, and 77.8 % of the differences are less than 1 ppmv (Fig. 2c). Approximately 5/6 of the data over the month show comparative stability. Similarly with HIPPO-1, the simulation results are always underestimates in the Southern Hemisphere and overestimates in the Northern Hemisphere. As shown in Fig. 2d, the complete simulation displays good performance, apart from one day in the Northern Hemisphere high latitudes. In the same manner, the RMSE shows good stability in the Southern Hemisphere, in particular for the low-to mid-latitudes of the Southern Hemisphere. The model also simulates well in the Northern Hemisphere, especially from 45 to 70° N.

Based on HIPPO-3 data from 24 March to 15 April 2010, the model simulation overestimates in March and underestimates in April. As shown in Fig. 2e, in March, the biases over several days were over 2 ppmv, and one of these days exceeded 3 ppmv. However, the absolute biases were all within 2 ppmv in April, and 75 % of the abso-





ACPD
15, 6745–6770, 2015



lute biases were less than 1 ppmv, which suggests relatively good performance by the model simulation. As shown by the RMSE, the data for the last days in March were not stable. However, 81.8 % of the data in April showed comparatively good stability. The absolute biases are all under 1.5 ppmv in the Southern Hemisphere, and are also within 2 ppmv for the low- and mid-latitudes of the Northern Hemisphere (Fig. 2f). However, a relatively large difference occurs at the Northern Hemisphere high latitudes, at one point exceeding 3 ppmv. Furthermore, the RMSE become greater with latitude from the Southern to Northern Hemisphere, inferring the simulation results are increasingly unstable with increasing latitude.

### 3.2 Validation of $CO_2$ vertical profiles

The GV flight plan performed 787 vertical ascents/descents from the ocean/ice surface/land surface to the tropopause. Two maximum altitude ascents were planned per flight to the tropopause/LS; one in the first half and the other in the second half of the research flight. In between, several vertical profiles from below the PBL to the mid-troposphere (1000–28 000 ft) were flown. Profiles were flown approximately every 2.2° of latitude with 4.4° between consecutive near-surface or high-altitude samples. Rate of climb and descent was 1500 ft $min^{-1}$ (457 m $min^{-1}$). During these profiles, the GV averaged a ground speed of approximately 175 m $s^{-1}$, or 10 km $min^{-1}$.

Most of a flight was conducted below the international Reduced Vertical Separation Minimum (RVSM), usually 29 000 ft or 8850 m, to allow the GV to descend and climb constantly to collect data at different altitudes throughout the troposphere. All flight plans were subject to modifications depending on local atmospheric conditions and approval by air traffic control. Most profiles extended from approximately 300 to 8500 m altitude, constrained by air traffic, but significant profiling extended above approximately 14 km.

One of the aims of this paper was to validate the model column-averaged concentration against the typical HIPPO flight plans, and we therefore examined the variability of $CO_2$ concentrations with HIPPO merged 10 s meteorology, atmospheric chemistry, and





ACPD
15, 6745–6770, 2015



aerosol measurements from Mission 1 to 3. For each mission, several hundred vertical profiles were produced. We have only selected the vertical profiles from near-surface to LS to compare the simulations using the standard model with observations. Each mission can be divided into six parts for analysis; the low-, mid- and high-latitudes in the Southern and Northern Hemispheres, respectively.

For HIPPO-1, the total simulation value is always less than the observation value in the Southern Hemisphere and vice versa in the Northern Hemisphere. The bias is less than 2 ppmv for the entire profile from the near-surface to the LS; however, it increases from 2 to 4 ppmv above 10 km covering the Northern Hemisphere high latitudes.

Figure 3 shows the comparison of simulation results and observations for data from the near-surface to the LS in the low-, mid- and high- latitude. In the low-latitudes, as shown by Fig. 3c and d, the simulation performed very well compared with observations. With the exception of the biases of approximately 2 ppmv in the tropopause in Fig. 3d, the biases are all within 1 ppmv. In the mid- and high-latitudes, it is different in both hemispheres. In the Southern Hemisphere, the majority biases are within 2 ppmv but the LS zone in Fig. 3a and 2 to 6 km region in Fig. 3b. In the Northern Hemisphere (Fig. 3e and f), the simulated vertical profiles show good performances, apart from UTLS, and the biases are less than 2 ppmv. Some large biases occurred in the UTLS exceeding 4 ppmv when the potential temperature gradient increased rapidly with height.

HIPPO-2 data showed overall similarity with HIPPO-1 data based on the distribution of positive and negative bias. However, an anomaly occurred at approximately −60° and 75° latitude, showing positive and negative biases, respectively, some exceeding 6 ppmv. Figure 4a is the vertical profile of the Southern Hemisphere high latitudes, which clearly shows that the simulation matches well with the observations from the near-surface to the tropopause. However, large biases occur above 8 km; Fig. 4b also shows this phenomenon above 10 km. In the low latitudes (Fig. 4c and d), the simulations match well with observations. The potential temperature gradient is smooth and the biases are less than 1 ppmv from near-surface to the UT, which indicates good





ACPD
15, 6745–6770, 2015



performance. For the mid-latitudes of the Northern Hemisphere, Fig. 4e shows relatively good simulation performance. However, as shown in Fig. 4f, the high latitudes did not perform well in the near-surface or the low- and mid-troposphere. Compared with observations, the simulation profiles do not appear to reflect the original shape.

As shown by HIPPO-3 data the biases increase abruptly with flight height for the mid- to high-latitudes of the Northern Hemisphere with values reaching 7 ppmv. In the high-latitudes of the Southern Hemisphere (Fig. 5a) the simulation underestimates the observations, and the absolute biases are isostatic from the near-surface to the LS, which are less than 3 ppmv. The Southern Hemisphere low latitudes (Fig. 5c) indicate good performance of the simulations, where all the biases are less than 1 ppmv. In the Northern Hemisphere low latitudes (Fig. 5d), the entire simulation appears to match well with observations. However, some locations do not reproduce the precise shape through the entire height. For the mid- to high- northern latitudes (Fig. 5e and f), the simulations performed relatively well from the near-surface to the UT. Larger bias in simulations is found in the winter lower stratosphere in the northern high-latitudes. The problem appears because between tropopause and 350 K level model uses vertical wind provided by reanalysis instead of using radiative heating rate, which is more accurate in stratosphere. The positive bias can reach level of 4 ppm for $CO_2$. This problem only affects simulations for observation made in lower stratosphere in high latitudes in cold season when the tropopause level is low. However the number of in-situ observations made in this altitude is very limited. The satellite observations of the total column such as GOSAT are also reduced considerably in high latitudes in cold season (Yoshida et al., 2013). Thus this lower stratosphere bias is not likely to deteriorate the transport model performance in the inverse modeling applications.

## 4 Conclusions

This study tested and verified the ability of a chemistry transport model to reproduce $CO_2$ vertical profiles using HIPPO merged 10 s meteorology, atmospheric chemistry,





ACPD
15, 6745–6770, 2015



and aerosol data from Missions 1 to 3, which span three different seasons (autumn, winter and spring). The results show that the model somewhat underestimates $CO_2$ in the Southern Hemisphere and overestimates it in the Northern Hemisphere for these three missions. However, the model was able to reproduce the seasonal and inter-annual variability of $XCO_2$ with RMS bias across all profiles with a level of 0.9 ppmv. The model performed well from the near-surface layer to the top of the troposphere, apart from the lower stratosphere the high latitude regions, in particular, in the Northern Hemisphere in spring, where large biases would often appear. The smaller bias of HIPPO-1 in January compared with HIPPO-3 in March and April arises from seasonal changes in meteorology and using the simplified fluxes, as mentioned in Patra et al. (2008).

The accuracy of these calculations will increase with the adaptation of the mass-balanced reanalysis data (MERRA, Bosilovich et al., 2008). Demand for global high-resolution fields of $CO_2$ and other greenhouse gases will also increase because of their use as a priori information in retrieval algorithms of observation instruments, such as the AIRS satellite (e.g., Strow and Hannon, 2008) and GOSAT (e.g., Yokota et al., 2009), and regional inverse modeling studies (Thompson et al., 2014).

*Acknowledgements.* The authors acknowledge the HIPPO data set available from CDIAC (ORNL). This project was supported by the National Basic Research Program of China (No. 2010CB951603). The computation was supported by the High Performance Computer Center of East China Normal University. We thank the team members of the Biogeochemical Cycle Modeling and Analysis Section of National Institute for Environment Studies, Tsukuba, Japan for providing expert advice and assistance. The GOSAT Level 4 data made available by GOSAT project (http://www.gosat.nies.go.jp/index_e.html).

## References

Baker, D. F., Law, R. M., Gurney, K. R., Rayner, P., Peylin, P., Denning, A. S., Bousquet, P., Bruhwiler, L., Chen, Y.-H., Ciais, P., Fung, I. Y., Heimann, M., John, J., Maki, T., Maksyutov, S., Masarie, K., Prather, M., Pak, B., Taguchi, S., and Zhu, Z.: TransCom 3 inversion





ACPD
15, 6745–6770, 2015



intercomparison: impact of transport model errors on the interannual variability of regional $CO_2$ fluxes 1988–2003, Global Biogeochem. Cy., 20, GB1002, doi:10.1029/2004GB002439, 2006.

Belikov, D., Maksyutov, S., Miyasaka, T., Saeki, T., Zhuravlev, R., and Kiryushov, B.: Mass-conserving tracer transport modelling on a reduced latitude-longitude grid with NIES-TM, Geosci. Model Dev., 4, 207–222, doi:10.5194/gmd-4-207-2011, 2011.

Belikov, D. A., Maksyutov, S., Sherlock, V., Aoki, S., Deutscher, N. M., Dohe, S., Griffith, D., Kyro, E., Morino, I., Nakazawa, T., Notholt, J., Rettinger, M., Schneider, M., Sussmann, R., Toon, G. C., Wennberg, P. O., and Wunch, D.: Simulations of column-averaged $CO_2$ and $CH_4$ using the NIES TM with a hybrid sigma-isentropic ($\sigma$–$\theta$) vertical coordinate, Atmos. Chem. Phys., 13, 1713–1732, doi:10.5194/acp-13-1713-2013, 2013.

Bolin, B. and Keeling, C. D.: Large scale atmospheric mixing as deduced from seasonal and meridional variations of the atmospheric carbon dioxide, J. Geophys. Res., 68, 3899–3920, 1963.

Bosilovich, M. G., Chen, J., Robertson, F. R., and Adler, R. F.: Evaluation of global precipitation in reanalysis, J. Appl. Meteorol. Clim., 47, 2279–2299, doi:10.1175/2008JAMC1921.1, 2008.

Bregman, B., Meijer, E., and Scheele, R.: Key aspects of stratospheric tracer modeling using assimilated winds, Atmos. Chem. Phys., 6, 4529–4543, doi:10.5194/acp-6-4529-2006, 2006.

Ciais, P., Sabine C., Bala G., Bopp L., Brovkin V., Canadell J., Chhabra A., DeFries R., Galloway J., Heimann M., Jones C., Le Quéré, C., Myneni R. B., Piao S., and Thornton P.: Carbon and Other Biogeochemical Cycles, in: Climate Change 2013: The Physical Science Basis. Contribution of Working Group I to the Fifth Assessment Report of the Intergovernmental Panel on Climate Change, edited by: Stocker, T. F., Qin, D., Plattner, G.-K., Tignor, M., Allen, S. K., Boschung, J., Nauels, A., Xia, Y., Bex, V., and Midgley, P. M., Cambridge University Press, Cambridge, United Kingdom and New York, NY, USA, 2013.

Dee, D. P. and Uppala, S.: Variational bias correction of satelliteradiance data in the ERA-Interim reanalysis, Q. J. Roy. Meteor. Soc., 135, 1830–1841, 2009.

Denning, A. S., Randall, D. A., Collatz, G. J., and Sellers, P. J.: Simulations of terrestrial carbon metabolism and atmospheric $CO_2$ in a general circulation model. II. Simulated $CO_2$ concentrations, Tellus B, 48, 543–567, doi:10.1034/j.1600-0889.1996.t01-1-00010.x, 1996.

Denning, A. S., Holzer, M., Gurney, K. R., Heimann, M., Law, R. M., Rayner, P. J., Fung, I. Y., Fan, S.-M., Taguchi, S., Friedlingstein, P., Balkanski, Y., Taylor, J., Maiss, M., and Levin, I.:





ACPD
15, 6745–6770, 2015



Three-dimensional transport and concentration of SF6: a model intercomparison study (TransCom2), Tellus B, 51, 266–297, 1999.
Douglass, A. R., Prather, M. J., Hall, T. M., Strahan, S. E., Rasch, P. J., Sparling, L. C., Coy, L., and Rodriguez, J. M.: Choosing meteorological input for the global modeling initiative assessment of high-speed aircraft, J. Geophys. Res., 104, 27545–27564, 1999.
GLOBALVIEW-$CO_2$: Cooperative Atmospheric Data Integration Project–Carbon Dioxide, CD-ROM, NOAA ESRL, Boulder, Colorado, 2010.
Gurney, K. R., Law, R. M., Denning, A. S., Rayner, P. J., Pak, B. C., Baker, D., Bousquet, P., Bruhwiler, L., Chen, Y. H., Ciais, P., Fung, I. Y., Heimann, M., John, J., Maki, T., Maksyutov, S., Peylin, P., Prather, M., and Taguchi, S.: Transcom 3 inversion intercomparison: model mean results for the estimation of seasonal carbon sources and sinks, Global Biogeochem. Cy., 18, GB1010, doi:10.1029/2003GB002111, 2004.
Hack, J. J., Boville, B. A., Briegleb, B. P., Kiehl, J. T., Rasch, P. J., and Williamson, D. L.: Description of the NCAR Community Climate Model (CCM2), NCAR/TN-382, 108, Climate and Global Dynamics Division, NCAR, Boulder, Colorado, USA, 1993.
Hall, T. M., Waugh, D. W., Boering, K. A., and Plumb, R. A.: Evaluation of transport in stratospheric models, J. Geophys. Res., 104, 18815–18839, 1999.
Hein, R., Crutzen, P. J., and Heimann, M.: An inverse modeling approach to investigate the global atmospheric methane cycle, Global Biogeochem. Cy., 11, 43–76, 1997.
Jacob, D., Prather, M. J., Rasch, P. J., Shea, R.-L., Balkanski, Y. J., Beagley, S. R., Bergmann, D. J., Blackshear, W. T., Brown, M., Chiba, M., Chipperfield, M. P., de Grandpré, J., Dignon, J. E., Feichter, J., Genthon, C., Grose, W. L., Kasibhatla, P. S., Köhler, I., Kritz, M. A., Law, K., Penner, J. E., Ramonet, M., Reeves, C. E., Rotman, D. A., Stockwell, D. Z., Van Velthoven, P. F. J., Verver, G., Wild, O., Yang, H., and Zimmermann, P.: Evaluation and intercomparison of global transport models using $^{222}$Rn and other short-lived tracers, J. Geophys. Res., 102, 5953–5970, 1997.
Jöckel, P., von Kuhlmann, R., Lawrence, M. G., Steil, B., Brenninkmeijer, C. A. M., Crutzen, P. J., Rasch, P. J., and Eaton, B.: On a fundamental problem in implementing flux-form advection schemes for tracer transport in 3-dimensional general circulation and chemistry transport models, Q. J. Roy. Meteor. Soc., 127, 1035–1052, 2001.
Keppel-Aleks, G., Wennberg, P. O., and Schneider, T.: Sources of variations in total column carbon dioxide, Atmos. Chem. Phys., 11, 3581–3593, doi:10.5194/acp-11-3581-2011, 2011.





ACPD
15, 6745–6770, 2015



Law, R. M., Peters, W., Rödenbeck, C., Aulagnier, C., Baker, I., Bergmann, D. J., Bousquet, P., Brandt, J., Bruhwiler, L., Cameron-Smith, P. J., Christensen, J. H., Delage, F., Denning, A. S., Fan, S.-M., Geels, C., Houweling, S., Imasu, R., Karstens, U., Kawa, S. R., Kleist, J., Krol, M., Lin, S.-J., Lokupitiya, R., Maki, T., Maksyutov, S., Niwa, Y., Onishi, R., Parazoo, N., Patra, P. K., Pieterse, G., Rivier, L., Satoh, M., Serrar, S., Taguchi, S., Takigawa, M., Vautard, R., Vermeulen, A. T., and Zhu, Z.: Trans Commodel simulations of hourly atmospheric $CO_2$: experimental overview and diurnal cycle results for 2002, Global Biogeochem. Cy., 22, GB3009, doi:10.1029/2007GB003050, 2008.

Mahowald, N. M., Plumb, R. A., Rasch, P. J., del Corral, J., and Sassi, F.: Stratospheric transport in a three-dimensional isentropic coordinate model, J. Geophys. Res., 107, 4254, doi:10.1029/2001JD001313, 2002.

Maksyutov, S., Patra, P. K., Onishi, R., Saeki, T., and Nakazawa, T.: NIES/FRCGC global atmospheric tracer transport model: description, validation, and surface sources and sinks inversion, Journal of the Earth Simulator, 9, 3–18, 2008.

Monge-Sanz, B. M., Chipperfield, M. P., Simmons, A. J., and Uppala, S. M.: Mean age of air and transport in a CTM: comparison of different ECMWF analyses, Geophys. Res. Lett., 34, L04801, doi:10.1029/2006GL028515, 2007.

Niwa, Y., Patra, P. K., Sawa, Y., Machida, T., Matsueda, H., Belikov, D., Maki, T., Ikegami, M., Imasu, R., Maksyutov, S., Oda, T., Satoh, M., and Takigawa, M.: Three-dimensional variations of atmospheric $CO_2$: aircraft measurements and multi-transport model simulations, Atmos. Chem. Phys., 11, 13359–13375, doi:10.5194/acp-11-13359-2011, 2011.

Onogi, K., Tsutsui, J., Koide, H., Sakamoto, M., Kobayashi, S., Hatsushika, H., Matsumoto, T., Yamazaki, N., Kamahori, H., Takahashi, K., Kadokura, S., Wada, K., Kato, K., Oyama, R., Ose, T., Mannoji, N., and Taira, R.: The JRA-25 reanalysis, J. Meteorol. Soc. Jap., 85, 369–432, 2007.

Parker, R., Boesch, H., Cogan, A., Fraser, A., Feng, L., Palmer, P. I., Messerschmidt, J., Deutscher, N., Griffith, D. W. T., Notholt, J., Wennberg, P. O., and Wunch, D.: Methane observations from the Greenhouse Gases Observing SATellite: comparison to ground based TCCON data and model calculations, Geophys. Res. Lett., 38, L15807, doi:10.1029/2011GL047871, 2011.

Patra, P. K., Baker, D., Bousquet, P., Bruhwiler, L., Chen, Y.-H., Ciais, P., Denning, S. A., Fan, S., Fung, I. Y., Gloor, M., Gurney, K., Heimann, M., Higuchi, K., John, J., Maki, T., Maksyutov, S., Peylin, P., Prather, M., Pak, B., Sarmiento, J., Taguchi, S., Takahashi, T., and Yuen, C.-W.:





ACPD
15, 6745–6770, 2015



Sensitivity of optimal extension of observation networks to the model transport, Tellus B, 55, 498–511, 2003a.

Patra, P. K., Maksyutov, S., Sasano, Y., Nakajima, H., Inoue, G., and Nakazawa, T.: An evaluation of $CO_2$ observations with Solar Occultation FTS for Inclined-Orbit Satellite sensor for surface source inversion, J. Geophys. Res., 108, 4759, doi:10.1029/2003JD003661, 2003b.

Patra, P. K., Peters, W., Rödenbeck, C., Aulagnier, C., Baker, I., Bergmann, D. J., Bousquet, P., Brandt, J., Bruhwiler, L., Cameron-Smith, P. J., Christensen, J. H., Delage, F., Denning, A. S., Fan, S.-M., Geels, C., Houweling, S., Imasu, R., Karstens, U., Kawa, S. R., Kleist, J., Krol, M., Law, R. M., Lin, S.-J., Lokupitiya, R., Maki, T., Maksyutov, S., Niwa, Y., Onishi, R., Parazoo, N., Pieterse, G., Rivier, L., Satoh, M., Serrar, S., Taguchi, S., Takigawa, M., Vautard, R., Vermeulen, A. T., and Zhu, Z.: TransCom model simulations of hourly atmospheric $CO_2$: analysis of synoptic-scale variations for the period 2002–2003, Global Biogeochem. Cy., 22, GB4013, doi:10.1029/2007GB003081, 2008.

Rasch, P. J., Boville, B. A., and Brasseur, G. P.: A three dimensional general circulation model with coupled chemistry for the middle atmosphere, J. Geophys. Res., 100, 9041–9071, 1995.

Raupach, M. R., Marland, G., Ciais, P., Le Quere, C., Canadell, J. G., Klepper, G., and Field, C. B.: Global and regional drivers of accelerating $CO_2$ emissions, P. Natl. Acad. Sci. USA, 104, 288–293, doi:10.1073/pnas.0700609104, 2007.

Rayner, P. J. and O'Brien, D. M.: The utility of remotely sensed $CO_2$ concentration data in surface inversion, Geophys. Res. Lett., 28, 175–178, 2001.

Rayner, P. J., Entiing, I. G., Francey, R. J., and Langenfelds, R.: Reconstructing the recent carbon cycle from atmospheric $CO_2$, $\delta^{13}C$ and $O_2/N_2$ observations, Tellus B, 51, 213–232, 1999.

Schoeberl, M. R., Douglass, A. R., Zhu, Z., and Pawson, S.: Acomparison of the lower stratospheric age spectra derived from a general circulation model and two data assimilation systems, J. Geophys. Res., 108, 4113, doi:10.1029/2002JD002652, 2003.

Scholes, R. J., Monteiro, P. M. S., Sabine, C. L., and Canadell, J. G.: Systematic long-term observations of the global carbon cycle, Trends Ecol. Evol., 24, 427–430, doi:10.1016/j.tree.2009.03.006, 2009.

Stohl, A., Cooper, O., and James, P.: A cautionary note on the use of meteorological analysis data for quantifying atmospheric mixing, J. Atmos. Sci., 61, 1446–1453, 2004.





ACPD
15, 6745–6770, 2015



Strow, L. L. and Hannon, S. E.: A 4-year zonal climatology of lower tropospheric $CO_2$ derived from ocean-only Atmospheric Infrared Sounder observations, J. Geophys. Res., 113, D18302, doi:10.1029/2007JD009713, 2008.

Tans, P., Fung, I., and Takahashi, T.: Observational constraints of the global atmospheric $CO_2$ budget, Science, 247, 1431–1438, 1990.

Thompson, R. L., Ishijima, K., Saikawa, E., Corazza, M., Karstens, U., Patra, P. K., Bergamaschi, P., Chevallier, F., Dlugokencky, E., Prinn, R. G., Weiss, R. F., O'Doherty, S., Fraser, P. J., Steele, L. P., Krummel, P. B., Vermeulen, A., Tohjima, Y., Jordan, A., Haszpra, L., Steinbacher, M., Van der Laan, S., Aalto, T., Meinhardt, F., Popa, M. E., Moncrieff, J., and Bousquet, P.: TransCom $N_2O$ model inter-comparison – Part 2: Atmospheric inversion estimates of $N_2O$ emissions, Atmos. Chem. Phys., 14, 6177–6194, doi:10.5194/acp-14-6177-2014, 2014.

Waugh, D. W. and T. M. Hall, Age of stratospheric air: Theory, observations, and models, Rev. Geophys., 40, 1010, doi:10.1029/2000RG000101, 2002.

Wunch, D., Toon, G., Blavier, J.-F. L., Washenfelder, R. A., Notholt, J., Connor, B. J., Griffith, D. W. T., Sherlock, V., and Wennberg, P. O.: The Total Carbon Column Observing Network (TCCON), Philos. T. R. Soc. A, 369, 2087–2112, doi:10.1098/rsta.2010.0240, 2011.

Yang, Z., Washenfelder, R. A., Keppel-Aleks, G., Krakauer, N. Y., Randerson, J. T., Tans, P. P., Sweeney, C., and Wennberg, P. O.: New constraints on Northern Hemisphere growing season net flux P, Geophys. Res. Lett., 34, 1–6, doi:10.1029/2007GL029742, 2007.

Yokota, T., Yoshida, Y., Eguchi, N., Ota, Y., Tanaka, T., Watanabe, H., and Maksyutov, S.: Global concentrations of $CO_2$ and $CH_4$ retrieved from GOSAT: first preliminary results, SOLA, 5, 160–163, doi:10.2151/sola.2009-041, 2009.

Yoshida, Y., Kikuchi, N., Morino, I., Uchino, O., Oshchepkov, S., Bril, A., Saeki, T., Schutgens, N., Toon, G. C., Wunch, D., Roehl, C. M., Wennberg, P. O., Griffith, D. W. T., Deutscher, N. M., Warneke, T., Notholt, J., Robinson, J., Sherlock, V., Connor, B., Rettinger, M., Sussmann, R., Ahonen, P., Heikkinen, P., Kyrö, E., Mendonca, J., Strong, K., Hase, F., Dohe, S., and Yokota, T.: Improvement of the retrieval algorithm for GOSAT SWIR $XCO_2$ and $XCH_4$ and their validation using TCCON data, Atmos. Meas. Tech., 6, 1533–1547, doi:10.5194/amt-6-1533-2013, 2013.





ACPD
15, 6745–6770, 2015



**Table 1.** Vertical grid levels of the NIES TM model.

| | $H$, km | $\sigma = P/P_s$ | $\approx \Delta$, m | $\xi$ ($\sigma$–$\theta$ grid levels), K | Number of levels |
|---|---|---|---|---|---|
| Near-surface layer | 0–2 | 1.0–0.795 | 250 | – | 8 |
| Free troposphere | 2–12 | 0.795–0.195 | 1000 | –, 330, 350, | 10 |
| Upper troposphere and stratosphere | 12–40 | 0.195–0.003 | 1000 | 365, 380, 400, 415, 435, 455, 475, 500, | 14 |
| | | | 2000 | 545, | |
| | | | – | 590, 665, 850, 1325, 1710 | |
| Total levels: 32 | | | | | |

$H$, height.
$P$, atmospheric pressure.
$P_s$, surface atmospheric pressure.
$\Delta$, vertical integral step.
$\xi$, the level of the sigma-isentropic grid.





ACPD
15, 6745–6770, 2015



**Table 2.** Temporal and spatial (horizontal) coverage of HIPPO mission flights.

| Missions | Sampling Dates | Vertical Profiles Flown | Flight Path Notes |
|---|---|---|---|
| HIPPO-1 | 8–30 Jan 2009 | 138 | Northern Polar flight #1 reached 80° N, Southern Ocean flight reached 67° S, 175° W (no return to the Arctic a second time) |
| HIPPO-2 | 31 Oct to 22 Nov 2009 | 148 | Northern Polar flight #1 reached 80° N, Southern Ocean flight reached 66° S, and 174° W, Northern Polar flight #2 reached 83° N |
| HIPPO-3 | 24 Mar to 16 Apr 2010 | 136 | Northern Polar flight #1 reached 84.75° N, Southern Ocean flight reached 66.8° S, 170° E, Northern Polar flight #2 reached 85° N |





ACPD
15, 6745–6770, 2015



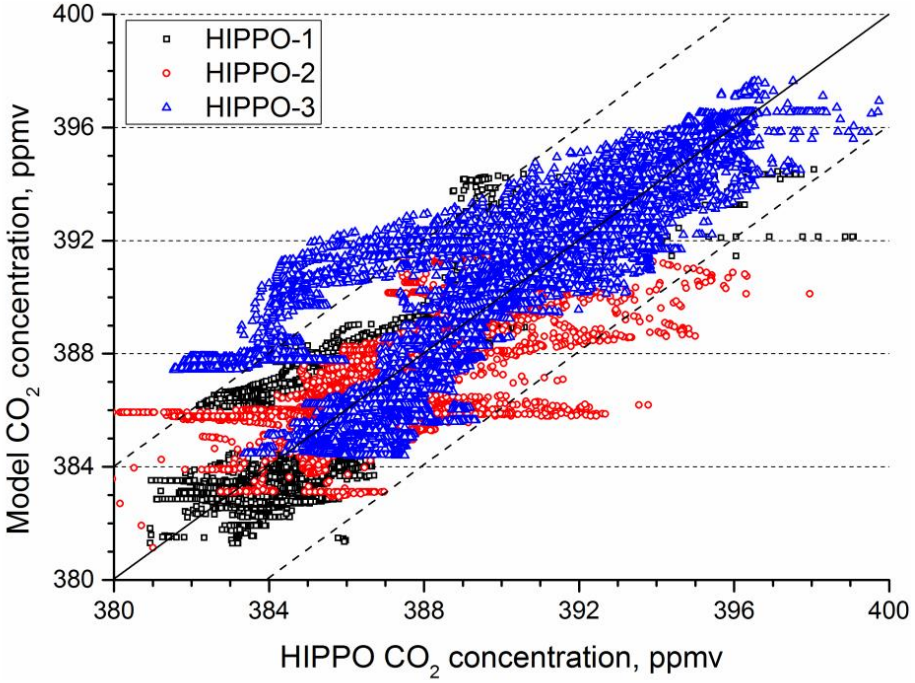


**Figure 1.** Scatter diagram of modeled and observed $CO_2$ of HIPPO-1 (black square), 2 (red circle), 3 (blue triangle). Dotted lines show a 95 % confidence interval of $CO_2$ concentration.





ACPD
15, 6745–6770, 2015



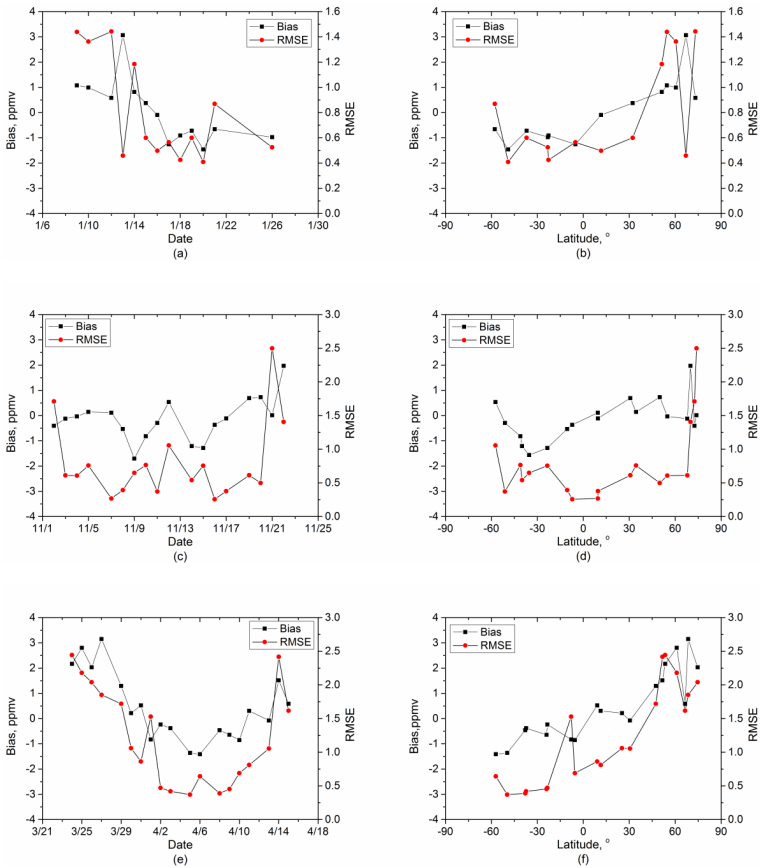


**Figure 2.** Bias (simulation-observation, black square) and RMSE (red circle) of time- (**(a)** HIPPO-1, **(c)** HIPPO-2, **(e)** HIPPO-3) and latitude-varying (**(b)** HIPPO-1, **(d)** HIPPO-2, **(f)** HIPPO-3) $CO_2$ concentration data.





ACPD
15, 6745–6770, 2015



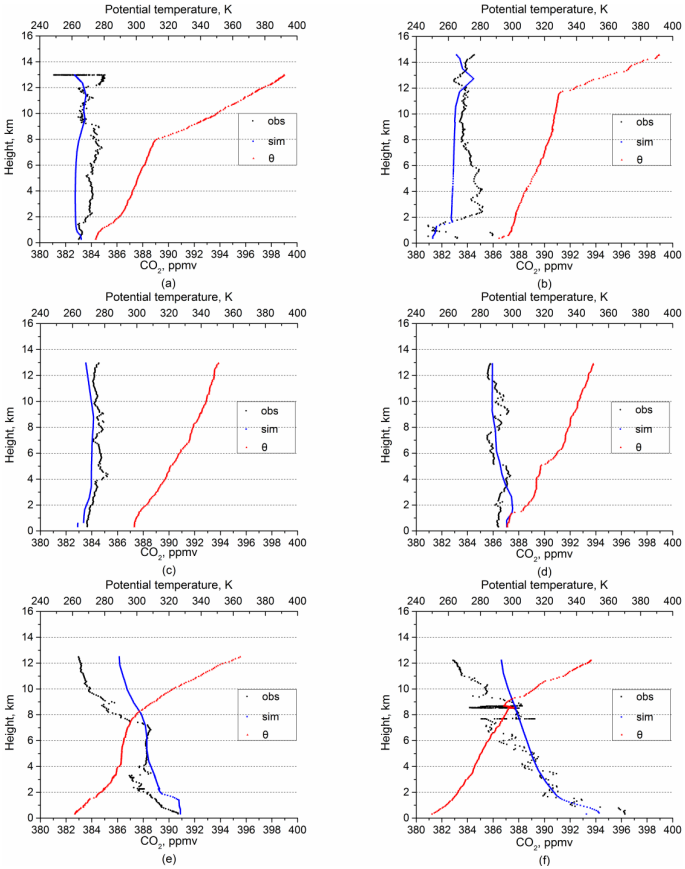


**Figure 3.** Vertical profiles from near-surface to the LS for HIPPO-1, panels represent the vertical profiles of observation (black square), simulation (blue square) and potential temperature (red square) in Southern (**(a)** high-, **(b)** mid-, **(c)** low- latitude), and Northern Hemisphere (**(d)** low-, **(e)** mid-, **(f)** high- latitude).





ACPD
15, 6745–6770, 2015



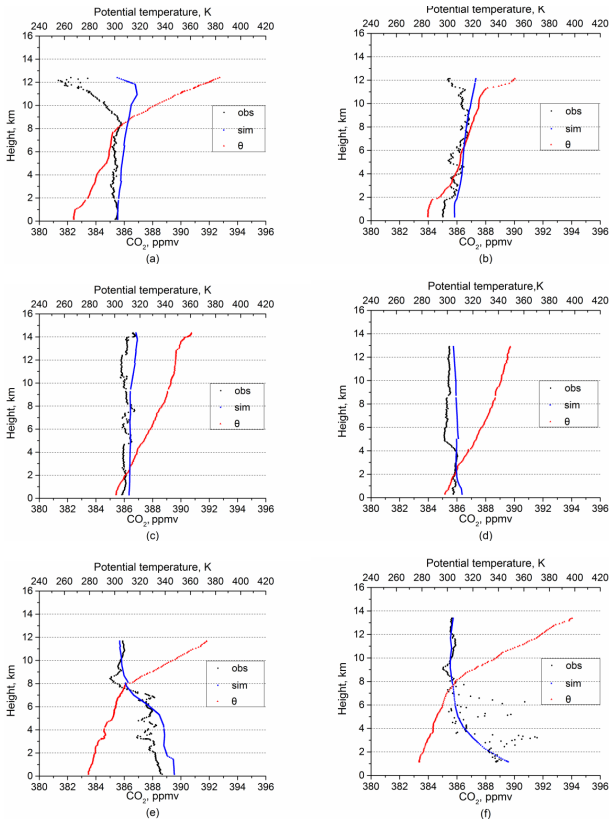


**Figure 4.** The vertical profiles from near-surface to the LS for HIPPO-2, panels represent the vertical profiles of observation (black square), simulation (blue square) and potential temperature (red square) in Southern (**(a)** high-, **(b)** mid-, **(c)** low- latitude), and Northern Hemisphere (**(d)** low-, **(e)** mid-, **(f)** high- latitude).





ACPD
15, 6745–6770, 2015



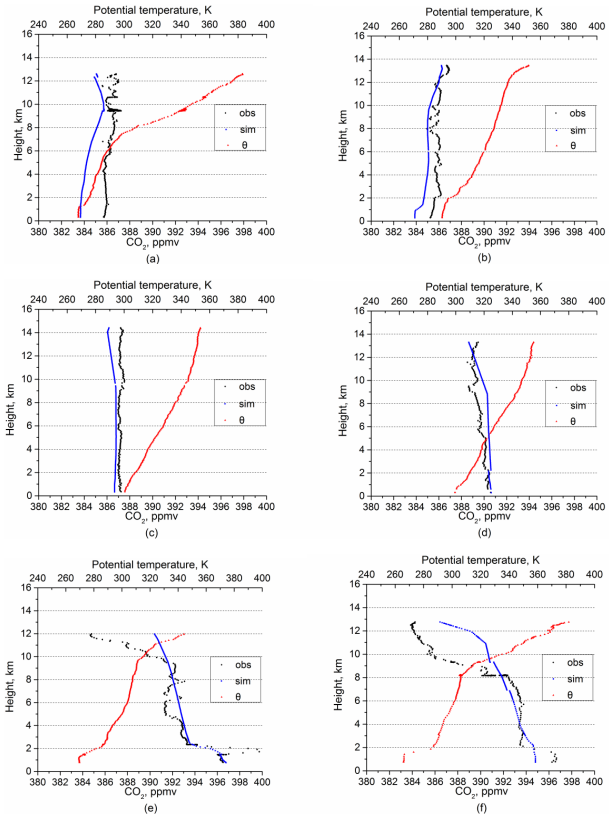


**Figure 5.** The vertical profiles from near-surface to the LS for HIPPO-3, panels represent the vertical profiles of observation (black square), simulation (blue square) and potential temperature (red square) in Southern (**(a)** high-, **(b)** mid-, **(c)** low- latitude), and Northern Hemisphere (**(d)** low-, **(e)** mid-, **(f)** high- latitude).





ACPD
15, 6745–6770, 2015